Chin. Phys. Lett. **39**, 047502 (2022)

Tunable Spin Hall Magnetoresistance in All-Antiferromagnetic Heterostructures

Lin Huang(黄琳), Yongjian Zhou(周永健), Tingwen Guo(郭庭温), Feng Pan(潘峰), and Cheng Song(宋成)*

Key Laboratory of Advanced Materials (MOE), School of Materials Science and Engineering, Tsinghua University, Beijing 100084, China

(Received 1 February 2022; accepted 11 March 2022; published online 28 March 2022)

We investigate the spin Hall magnetoresistance (SMR) in all-antiferromagnetic heterostructures α-Fe_2O_3/Cr_2O_3 with Pt contacts. When the temperature is ultralow (<50 K), the spin current generated in the Pt layer cannot be transmitted through Cr_2O_3 ($t = 4$ nm), and the SMR is near zero. Meanwhile, when the temperature is higher than the spin fluctuation temperature T_F (≈ 50 K) of Cr_2O_3 and lower than its Néel temperature T_N (≈ 300 K), the spin current goes through the Cr_2O_3 layer and is reflected at the α-Fe_2O_3/Cr_2O_3 interface; an antiferromagnetic (negative) SMR is observed. As temperature increases higher than T_N, paramagnetic (positive) SMR mainly arises from the spin current reflection at the Cr_2O_3/Pt interface. The transition temperatures from negative to positive SMR are enhanced with increasing Cr_2O_3 layer thickness, accompanied by the absence of SMR signals when $t = 10$ nm. Such a tunable SMR builds a bridge between spin transport and structures. It also enriches antiferromagnetic spintronics.

DOI: 10.1088/0256-307X/39/4/047502

Spin transport at magnet/heavy metal (HM) bilayers provides a rich platform for spintronics.[1] The spin Hall magnetoresistance (SMR) effect is a phenomenon in which the resistance of the HM layer depends on the angle between the spin polarization σ of spin current and the magnetic order M of magnetic layers. When σ is perpendicular (parallel) to M, the resistance is high (low) because of the absorption (reflection) of spin current at the interface.[2–6] Next, the SMR in antiferromagnet/HM is negative because of the spin-flop transition (Néel order is perpendicular to the magnetic field above a critical field). The introduction of an additional magnetic layer would enrich or complicate the spin transport. A sign change in SMR was observed in ferromagnetic insulators (FMIs) YIG (or γ-Fe_2O_3)/Pt bilayers by inserting an antiferromagnetic insulator (AFI) NiO,[3,7–10] revealing the magnon spin current transmission through AFI and spin current reflection at the FMI/AFI interface. In $Y_3Fe_5O_{12}$ (YIG)/Cr_2O_3/Pt heterostructures,[11] the spin conducting and non-conducting states are modulated by the spin structure of Cr_2O_3. Meanwhile, in YIG/NiO/YIG structures, the SMR response depends on the orientation of two YIG magnetizations (parallel or antiparallel).[12] However, whether the sign of SMR can be modulated in all-antiferromagnetic heterostructures has not been reported.

In this Letter, we experimentally investigate the temperature-dependent SMR in α-Fe_2O_3/Cr_2O_3/Pt heterostructures. Here α-Fe_2O_3 is an AFI with an easy plane (0001) at room temperature. In bulk, it exhibits a Néel temperature of $T_N = 953$ K with the Morin transition at $T \approx 263$ K.[13] The α-Fe_2O_3/Pt bilayer exhibits a large negative SMR.[14,15] Cr_2O_3 is a prototypical AFI with out-of-plane uniaxial anisotropy and $T_N \approx 307$ K.[16,17] The experiments investigate the SMR variation as a function of temperature and Cr_2O_3 thickness in all-antiferromagnetic heterostructures.

The epitaxial α-Fe_2O_3 (4 nm)/Cr_2O_3 (t nm) bilayers were fabricated on Al_2O_3 (0001) substrates through pulsed laser deposition from Fe_2O_3 and Cr_2O_3 targets. The pulsed laser source employed a KrF laser of 248 nm wavelength. The laser energy density was kept at 3 J/cm^2 with a repetition rate of 2 Hz and 3 Hz for α-Fe_2O_3 and Cr_2O_3, respectively. The base pressure of the chamber before deposition was less than 3×10^{-5} Pa. The deposition temperature was 450 ℃ in an oxygen atmosphere of 2.67 Pa. Additionally, the epitaxial growth is confirmed through *in situ* reflection high-energy electron diffraction (RHEED). The films were cooled down to room temperature after deposition at the rate of 10 ℃/min under the oxygen pressure of 2×10^4 Pa. Then, a 5-nm-thick Pt layer was grown on the surface of the Cr_2O_3 film by magnetron sputtering, where the base pressure of the chamber was less than 6×10^{-7} Pa. The film roughness was measured by an atomic force microscope. The qualities of films were characterized by x-ray diffraction (XRD). The cross-section imaging was performed

*Corresponding author. Email: songcheng@mail.tsinghua.edu.cn
© 2022 Chinese Physical Society and IOP Publishing Ltd

on a high-resolution transmission electron microscopy (HRTEM). Finally, a Hall bar of 500 μm ×50 μm was patterned for electrical measurements by photolithography and Ar ion beam etching.

Figure 1(a) shows typical RHEED images of α-Fe_2O_3 and Cr_2O_3 surfaces. The RHEED pattern of the α-Fe_2O_3 and Cr_2O_3 surfaces is streaky, indicating a flat surface of the bilayer. According to the structure factor of the corundum structure, $[11\bar{2}0]$ projected reciprocal lattice of the single-crystalline corundum (0001) surface is asymmetric.[18] Figure 1(b) shows an XRD result of α-Fe_2O_3/Cr_2O_3 on the Al_2O_3 (0001) substrate, where peaks (0006) of α-Fe_2O_3 and Cr_2O_3 can be seen at 39.5° and 40.1°, respectively. The latter is next to the Al_2O_3 (0001) substrate peak. Figure 1(c) shows the surface topography of the bilayer using atomic force microscopy, exhibiting a flat surface with a small surface roughness of 0.18 nm. Figure 1(d) shows a typical cross-sectional HRTEM image of α-Fe_2O_3/Cr_2O_3/Pt cross section. Therefore, the surface of the bilayer is relatively smooth, which is essential to grow a high-quality top layer of heavy-metal Pt on it.

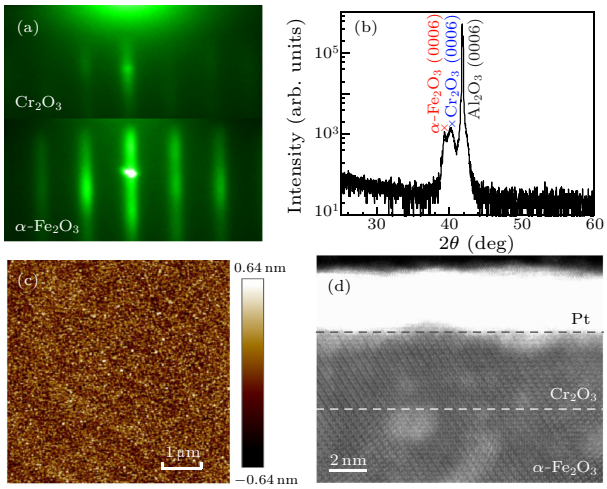

Fig. 1. (a) RHEED patterns of α-Fe_2O_3 and Cr_2O_3 surfaces. (b) XRD spectra of α-Fe_2O_3/Cr_2O_3 grown on the Al_2O_3 (0001) substrate. (c) Atomic force microscopy image of α-Fe_2O_3/Cr_2O_3 surface with a roughness of 0.18 nm. (d) HRTEM image of the α-Fe_2O_3/Cr_2O_3/Pt cross section.

We now investigate the SMR responses in α-Fe_2O_3 (4 nm)/Cr_2O_3 (4 nm)/Pt heterostructure at temperatures ranging from 10 K to 350 K. Figure 2(a) shows the schematics of the Hall bar with in-plane rotation angle α defined between the external magnetic field $\boldsymbol{H}$ and x-axis in the xy plane. The external magnetic field H is 50 kOe, which is sufficient for the spin-flop transition (several thousands of Oe) of α-Fe_2O_3.[14,15,19,20] The xy plane is the film plane, where the current J_e is applied along the x-axis. The magnetoresistance (MR) is calculated as the change in resistance $\Delta R_{xx} = R_{xx} - R_{\min}$ and normalized to the resistance $\Delta R_{xx}/R_{\min}$, where $R_{\min}$ is the minimum resistance during the magnetic field rotation from 0° to 360°. Figure 2(b) shows the SMR responses in α-Fe_2O_3 (4 nm)/Cr_2O_3 (4 nm)/Pt heterostructure as a function of angle α with different temperatures. At ultralow temperature (T = 10 K), the Néel order of Cr_2O_3 is aligned out-of-plane, the spin current is blocked, and SMR is nearly zero. Next, when the temperature ranges from 50 K to 200 K, the SMR curve shows $[1 - \cos(2\alpha)]$ angle dependence, featured as M-shape, and the maximum resistance appears at α = 90° and 270°. The M-shape SMR arises from the spin current reflected at α-Fe_2O_3/Cr_2O_3 interface, which is quite characteristic of the antiferromagnetic α-Fe_2O_3. The spin current can be transmitted through the Cr_2O_3 layer when the Cr_2O_3 magnetic moment is in the magnetic fluctuation state with temperatures ranging from 50 K to 200 K. When the temperature is higher ($T \geq$ 300 K), SMR shows a $\cos(2\alpha)$ angular-dependent behavior, and the maximum resistance appears at α = 0° and 180°, which is considered as W-shape. The W-shape SMR arises from the spin current reflected at Cr_2O_3/Pt interface, where Cr_2O_3 is in the paramagnetic phase.[21–23]

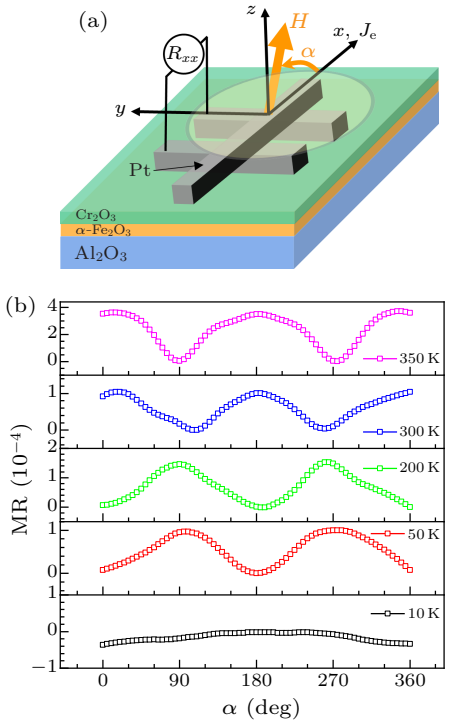

Fig. 2. (a) Schematic of in-plane α angular dependence of magnetoresistance in α-Fe_2O_3 (4 nm)/Cr_2O_3 (4 nm)/Pt. The magnetic field $\boldsymbol{H}$ is rotated in the xy plane with angles α relative to the x-axis, and charge current J_e is applied along the x direction. (b) In-plane α angular-dependent magnetoresistance measured with magnetic field H = 50 kOe for various temperatures (marked in the figure) for the α-Fe_2O_3 (4 nm)/Cr_2O_3 (4 nm)/Pt sample.

For comparison, the SMR responses of α-Fe_2O_3 (4 nm)/Pt [Fig. 3(a)] and Cr_2O_3 (4 nm)/Pt bilayer

[Fig. 3(b)] were measured with a temperature ranging from 10 K to 350 K. The measuring method and device geometry are identical with Fig. 2(a). As shown in Fig. 3(a), the SMR signal of α-Fe_2O_3/Pt bilayer exhibits an M-shape. The maximum resistance appears at 90° and 270°, where the Néel vector $\boldsymbol{n}$ is coplanar with charge current J_e and $\boldsymbol{H}$, and perpendicular to the in-plane magnetic field $\boldsymbol{H}$.[24–26] As the temperature increases from 10 K to 350 K, the magnitude of the SMR signal increases because the spin-orbit coupling of Pt is stronger at higher temperatures.[27] As shown in Fig. 3(b), the SMR signal shows a W-shape when $T > T_N$ ($\approx$ 300 K), originating from the paramagnetic state of Cr_2O_3. This paramagnetic polarization of Cr_2O_3 will always follow the large external magnetic field, producing a positive SMR.[21,28,29] The situation differs dramatically when the sample is cooled below the Néel temperature; the signals become almost constant without a typical SMR shape (T = 200, 50, and 10 K). In this scenario, the Néel order of Cr_2O_3 is aligned out of plane, producing no SMR signal.

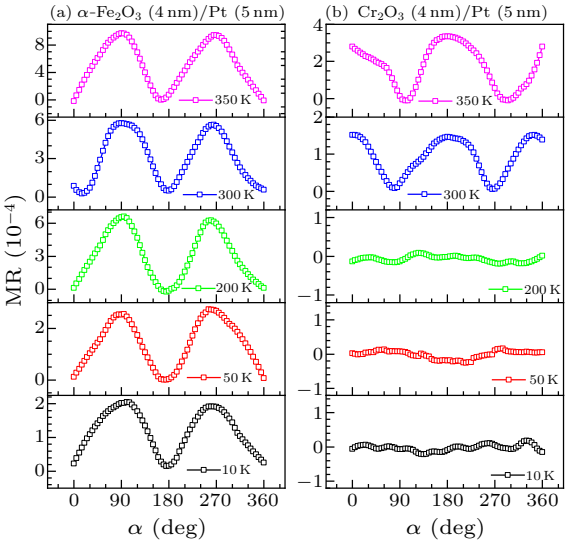

Fig. 3. The α-dependent magnetoresistance measured with magnetic field H = 50 kOe for various temperatures in (a) α-Fe_2O_3 (4 nm)/Pt and (b) Cr_2O_3 (4 nm)/Pt bilayers.

Figure 4(a) shows the temperature-dependent SMR ratio of α-Fe_2O_3 (4 nm)/Cr_2O_3 (t nm)/Pt with different Cr_2O_3 thicknesses t (t = 0, 2, 4, 6, and 10 nm). The SMR ratio is defined as SMR ratio = $(R_0 - R_{90})/R_0$; here, R_0 and R_{90} denote the resistance value at α = 0° and 90°, respectively. When the temperature (T = 10 K) is lower than T_N, the Néel vector of Cr_2O_3 is along the easy axis (out-of-plane), the spin current cannot be transmitted through Cr_2O_3, and no SMR signal is observed when $t \geq$ 4 nm. Moreover, when the temperature is between 50 K and 200 K ($0 < t \leq$ 4 nm), the negative M-shape SMR is observed, and the Néel vector of Cr_2O_3 is in a magnetic fluctuation state. The uniaxial anisotropy of Cr_2O_3 reduces as temperature increases, resulting in the inclination of the Néel vector when magnons are excited and enabling the spin current transportation with an in-plane component of the spin polarization. Phenomenologically, we define the fluctuation temperature T_F based on the negative SMR that appears. The spin current transmitted through the Cr_2O_3 layer is reflected at the α-Fe_2O_3/Cr_2O_3 interface, as shown in the schematic in the inset (i) of Fig. 4(a). As the temperature increases higher than T_N and Cr_2O_3 is in the paramagnetic phase, a positive W-shape SMR is observed with the thickness t = 2, 4, and 6 nm. The paramagnetic state of Cr_2O_3 follows the external magnetic field, and positive SMR mainly arises from the spin current reflection at the Cr_2O_3/Pt interface, instead of the α-Fe_2O_3/Cr_2O_3 interface shown in the inset (ii) of Fig. 4(a). Figure 4(b) shows the temperature-dependent SMR ratio of Cr_2O_3/Pt bilayers with different thicknesses. Positive SMR is observed in the paramagnetic phase of Cr_2O_3 with t = 2 and 4 nm; however, it vanishes when cooling below the Néel temperature. Meanwhile, the SMR signal is absent in the bilayers when t is thicker (t = 6 and 10 nm). The results show that the spin current can be transmitted through Cr_2O_3 with thinner thicknesses, and the transmittance of the spin current decreases as the thickness of Cr_2O_3 increases.

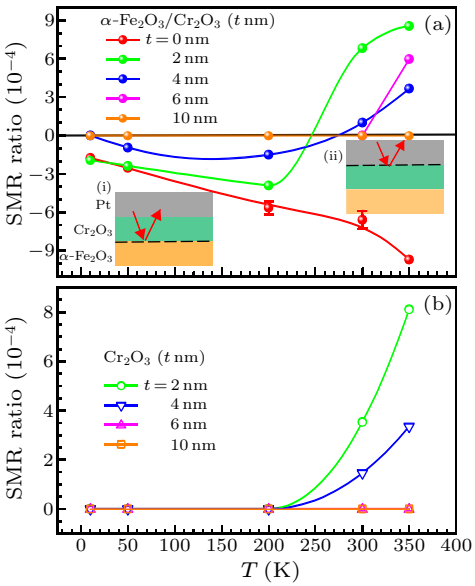

Fig. 4. (a) SMR ratio of α-Fe_2O_3 (4 nm)/Cr_2O_3 (t nm)/Pt as a function of temperature with t = 0, 2, 4, 6, and 10 nm. (b) SMR ratio of Cr_2O_3 (t nm)/Pt as a function of temperature with t = 2, 4, 6, and 10 nm.

The experimental results show that the spin current could only be transmitted if its polarization direction is parallel or antiparallel to the Néel order of Cr_2O_3. When the temperature is ultralow ($T < T_F$), the polarization of spin current is perpendicular to the

Néel vector of Cr_2O_3, and no MR response is observed where the spin current cannot be transmitted through Cr_2O_3 [Fig. 5(a)]. Meanwhile, when $T_F < T < T_N$, a negative M-shape SMR is observed, in which the spin current transmits through Cr_2O_3 and reflects from the bottom α-Fe_2O_3/Cr_2O_3 interface [Fig. 5(b)]. As the temperature increases higher than the Néel temperature ($T > T_N$), due to the spin current reflection from the Cr_2O_3/Pt interface, a positive W-shape SMR is observed [Fig. 5(c)].

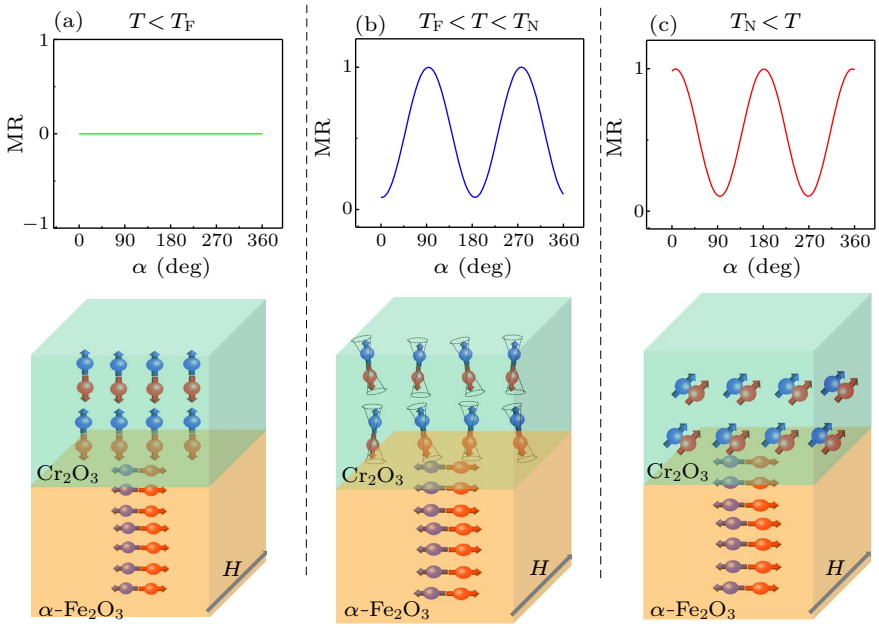

Fig. 5. Illustrations for the magnetic structures and spin current transportation in α-Fe_2O_3/Cr_2O_3/Pt with temperature variation. (a) $T < T_F$, the two Néel vectors (Cr_2O_3 and α-Fe_2O_3) are perpendicular. (b) $T_F < T < T_N$, the Néel vector of Cr_2O_3 is in the magnetic fluctuation state, and spin current can be transmitted through the in-plane components of Cr_2O_3. (c) $T > T_N$, magnetic order of Cr_2O_3, and Néel vector of α-Fe_2O_3 are perpendicular.

In summary, we have investigated the SMR response in α-Fe_2O_3/Cr_2O_3/Pt heterostructures with varying temperatures and Cr_2O_3 thicknesses t. As the temperature changes for $t = 2$ and 4 nm, we observed a sign change in SMR, which can be explained by the spin current reflection at α-Fe_2O_3/Cr_2O_3 interface when the temperature ranges from T_F to T_N (negative SMR) and spin current reflection at the Cr_2O_3/Pt interface when the temperature is higher than T_N (positive SMR). The spin current cannot be transmitted when Cr_2O_3 is thick ($t = 6$ and 10 nm), and only a positive SMR signal is observed at high temperature ($T > T_N$). Our results provide a potential advantage for distinguishing the source of spin flow in the signal in multilayer heterostructures and highlight the importance of magnetic structure (Néel vector) in AFI, which opens the possible way to manipulate the spin current transportation and AFI memory device.[30]

Acknowledgments. This work was supported by the National Key R&D Program of China (Grant No. 2021YFB3601301), the National Natural Science Foundation of China (Grant No. 51871130), the Natural Science Foundation of Beijing Municipality (Grant No. JQ20010). We acknowledge the support of Beijing Innovation Center for Future Chip, Tsinghua University.

References

[1] Hellman F *et al.* 2017 *Rev. Mod. Phys.* **89** 025006
[2] Nakayama H, Althammer M, Chen Y T, Uchida K, Kajiwara Y, Kikuchi D, Ohtani T, Geprägs S, Opel M, Takahashi S, Gross R, Bauer G E W, Goennenwein S T B and Saitoh E 2013 *Phys. Rev. Lett.* **110** 206601
[3] Hou D, Qiu Z, Barker J, Sato K, Yamamoto K, Vélez S, Gomez-Perez J M, Hueso L E, Casanova F and Saitoh E 2017 *Phys. Rev. Lett.* **118** 147202
[4] Zhao Z P, Guo Q, Chen F H, Zhang K W and Jiang Y 2021 *Rare Met.* **40** 2862
[5] Chen Y, Takahashi S, Nakayama H, Althammer M, Goennenwein S T B, Saitoh E and Bauer G E W 2013 *Phys. Rev. B* **87** 144411
[6] Zhang X, Luo T, Hu X, Guo J, Lin G, Li Y, Liu Y, Zhang X, Luo T, Hu X, Guo J, Lin G, Li Y, Liu Y, Li X, Ge J, Xing Y, Zhu Z, Gao P, Sun L and Wang J 2019 *Chin. Phys. Lett.* **36** 057402
[7] Shang T, Zhan Q F, Yang H L, Zuo Z H, Xie Y L, Liu L P, Zhang S L, Zhang Y, Li H H, Wang B M, Wu Y H, Zhang S and Li R W 2016 *Appl. Phys. Lett.* **109** 032410
[8] Baldrati L, Ross A, Niizeki T, Schneider C, Ramos R, Cramer J, Gomonay O, Filianina M, Savchenko T, Heinze D, Kleibert A, Saitoh E, Sinova J and Kläui M 2018 *Phys. Rev. B* **98** 024422
[9] Lin W and Chien C L 2017 *Phys. Rev. Lett.* **118** 067202
[10] Dong B, Baldrati L, Schneider C, Niizeki T, Ramos R, Ross A, Cramer J, Saitoh E and Kläui M 2019 *Appl. Phys. Lett.* **114** 102405
[11] Qiu Z, Hou D, Barker J, Yamamoto K, Gomonay O and Saitoh E 2018 *Nat. Mater.* **17** 577

[12] Guo C Y, Wan C H, He W Q, Zhao M K, Yan Z R, Xing Y W, Wang X, Tang P, Liu Y Z, Zhang S, Liu Y W and Han X F 2020 *Nat. Electron.* **3** 304
[13] Morin F J 1950 *Phys. Rev.* **78** 819
[14] Zhou Y J, Chen X Z, Zhou X F, Bai H, Chen R Y, Pan F and Song C 2020 *J. Appl. Phys.* **127** 163904
[15] Fischer J, Althammer M, Vlietstra N, Huebl H, Goennenwein S T B, Gross R, Geprägs S and Opel M 2020 *Phys. Rev. Appl.* **13** 014019
[16] Kosub T, Kopte M, Radu F, Schmidt O G and Makarov D 2015 *Phys. Rev. Lett.* **115** 097201
[17] Kosub T, Kopte M, H€U R, Appel P, Shields B, Maletinsky P, Hübner R, Liedke M O, Fassbender J, Schmidt O G and Makarov D 2017 *Nat. Commun.* **8** 13985
[18] Moriyama T, Shiratsuchi Y, Iino T, Aono H, Suzuki M, Nakamura T, Kotani Y, Nakatani R, Nakamura K and Ono T 2020 *Phys. Rev. Appl.* **13** 034052
[19] Morrish A H 1994 *Canted Antiferromagnetism: Hematite* (Singapore: World Scientific)
[20] Ross A, Lebrun R, Ulloa C, Grave D A, Kay A, Baldrati L, Kronast F, Valencia S, Rothschild A and Kläui M 2020 *Phys. Rev. B* **102** 094415
[21] Schlitz R, Kosub T, Thomas A, Fabretti S, Nielsch K, Makarovand D and Goennenwein S T B 2018 *Appl. Phys. Lett.* **112** 132401
[22] Corliss L M, Hastings J M, Nathans R and Shirane G 1965 *J. Appl. Phys.* **36** 1099
[23] Pisarev R V, Krichevtsov B B and Pavlov V V 1991 *Phase Transit.* **37** 63
[24] Huang L, Zhou Y, Qiu H S, Guo T, Pan F, Jin B and Song C 2021 *Appl. Phys. Lett.* **119** 212401
[25] Cheng Y, Yu S S, Ahmed A S, Zhu M L, Rao Y, Ghazisaeidi M, Hwang J and Yang F Y 2019 *Phys. Rev. B* **100** 220408
[26] Chen X, Shi S, Shi G, Fan X, Song C, Zhou X, Bai H, Liao L, Zhou Y, Zhang H, Li A, Chen Y, Han X, Jiang S, Zhu Z, Wu H, Wang X, Xue D, Yang H and Pan F 2021 *Nat. Mater.* **20** 800
[27] Chen S, Li D, Cui B, Xi L, Si M, Yang D and Xue D 2018 *J. Phys. D: Appl. Phys.* **51** 095001
[28] Althammer M, Meyer S, Nakayama H, Schreier M, Altmannshofer S, Weiler M, Huebl H, Geprägs S, Opel M, Gross R, Meier D, Klewe C, Kuschel T, Schmalhorst J M, Reiss G, Shen L, Gupta A, Chen Y T, Bauer G E W, Saitoh E and Goennenwein S T B 2013 *Phys. Rev. B* **87** 224401
[29] Aqeel A, Vlietstra N, Heuver J A, Bauer G E W, Noheda B, van Wees B J and Palstra T T M 2015 *Phys. Rev. B* **92** 224410
[30] Wang Y, Zhu D, Yang Y, Lee K, Mishra R, Go G, Oh S H, Kim D H, Cai K, Liu E, Pollard S D, Shi S, Lee J, Teo K L, Wu Y, Lee K J and Yang H 2019 *Science* **366** 1125